



INFLUENCE OF PLASMA GAS FLOW RATE ON THE MECHANICAL AND MICROSTRUCTURAL ASPECTS OF PLASMA ARC WELDED TITANIUM ALLOY JOINTS

Pragatheswaran T, *Rajakumar S and Balasubramanian V

Annamalai University, Annamalai Nagar, Tamil Nadu- 608002, India

ABSTRACT

In the present investigation, the effect and role of plasma gas flow rate on the formation of microstructure during plasma arc welding of Ti₆Al₄V titanium alloy were studied using microscopic observation, energy dispersive spectroscopic analysis, tensile tests and microhardness measurements. Plasma gas flow rate influences the arc pressure, arc constriction, and stability. The transformation of plasma arc from conduction mode to keyhole mode causes severe changes to the microstructural characteristics of the titanium welds. This transformation takes place with slight variations of PGFR. Weld geometries increase with an increase in the PGFR. The microstructural examination shows that there are various phases formed during the variation in PGFR. Fusion zone had acicular α and widmanstätten α . Mechanical properties (i.e) strength and hardness of the joints increase with an increase in plasma gas flow rate. In the joint welded with 1 L/min, there is the formation of α -case which is an oxygen rich brittle subsurface structure and found detrimental to the ductility of the joints.

Keywords: Plasma arc welding, Titanium alloy Microstructure, Defects and Tensile Strength

1. Introduction

Titanium and its alloys possess very attractive characteristics which include higher specific strength and lower density compared to most of the structural steels in practice [1]. The classification of titanium alloys is based on their composition. Ti₆Al₄V is commercially used in wide a perspective because of its combination of good strength, formability and weldability. The most important components that are made using this alloy are the pressure vessels, aero-engine components such as compressor blades, rotor and stator components, engine shrouds, etc. [2]. Titanium has a high affinity for oxygen at high temperatures, resulting in rapid oxidation. [3-6]. Although there are other welding processes available, Gas Tungsten Arc Welding (GTAW) is the most often used technique for welding titanium alloys because of its cost-effectiveness. The problems associated with the welding of titanium alloys can be identified based on the process characteristics and material characteristics themselves [7,8].

High capitalization cost and selective environments require high energy density welding processes like laser beam or electron beam welds. Plasma arc welding (PAW) is similar to GTAW in that both techniques produce the welding arc with a non-consumable

tungsten electrode. The major difference between the two processes is that there is an additional inert gas supply (mostly high purity argon) which is consumed to produce the arc with high energy density. When compared to other fusion welding methods, the high energy density of the arc produced by PAW produces better weld properties. [9,10]. The important process parameters which govern the welding characteristics in PAW are the welding current, welding speed, plasma gas flow rate and arc length (stand-off distance). Among the various process parameters of PAW, the plasma gas flow rate (PGFR) plays a vital role in determining the weld characteristics of titanium alloys [11,12]. PGFR is a predominant parameter along with welding current, which influences the formation of weld with conduction mode or keyhole mode plasma. The formation of weld caused by the deposition of arc energy is called conduction mode plasma arc welding. The keyhole mode of welding was developed by the formation of a hole which cuts the root of the weld and is subsequently filled with the material which precedes [13]. The welding arc that is transmitted from the electrode is concentrated on the workpiece surface by the virtue of applying a plasma gas. The rate at which the plasma gas is applied through the welding arc caused it to concentrate like a beam which is usually observed as a cylindrical column of the welding arc. J. Chen et al. [14] experimented with the keyhole plasma arc welding of titanium alloy with a pulse dynamic controlling

*Corresponding Author - E- mail: srkcemajor@yahoo.com

technique in which an attempt was made to reduce the application of excess heat input without losing the keyhole formation that is confirmed by the presence of efflux plasma in the under-bead surface. Keyholing can be controlled by the process parameters in plasma arc welding of thin sheets which was presented by W. Sun et al. [15] and numerical analysis was performed by A. Deshpande et al. [16]. Titanium alloys have unique microstructural properties that respond differently to welding processes and composition. The most desirable characteristic microstructure is the prior β grain structure. The heat input of the welding process reflects directly on the prior β grain size and width of the weld bead. During welding of titanium, the transformation of β occurs from liquidus temperature to various phases such as α and α' which are bounded by the grain boundary β phase [17,18]. Thus, the transformation kinetics of β to α and α' is primarily controlled by the cooling rate. The titanium alloy's microstructure has surface and subsurface properties that are influenced by heating and cooling cycles and compositional changes during welding. [19-23]. The characteristics of phases developed during cooling determine the properties of the welded joints.

The brief literature analysis provided enough impetus to investigate the impact of one of the most critical PAW process parameters, plasma gas flow rate, on the microstructural and mechanical properties of welded titanium alloy joints. In this investigation, Ti6Al4V alloy thin sheets are welded using plasma arc welding process and the efforts are put to evaluate the defects such as porosity, weld geometry using optical image analysis and associated mechanical properties using tensile test and hardness test, microstructural characteristics by optical and scanning electron microscopy and elemental composition by energy dispersive spectroscopy (EDS).

2. Materials and Methods

The base material used in this investigation is the Ti6Al4V alloy commercially called Grade 5 Titanium alloy (Al – 6.12%, V – 4.14%, Fe – 0.01%, C- 0.03%, O – 0.15%, N – 0.01%, H – 0.003%). The microstructure of the base material is characterized by equiaxed α grains bounded by granular β grains and are shown in Figure 1.

The dimension of the specimen prepared for welding is $120 \times 60 \times 2$ mm³ blanks which are cut using wire cut electric discharge machining (EDM). Contamination is a key concern in specimen preparation of titanium alloys because of their strong affinity for oxygen, which causes extra attention to the metal's

cleanliness. Hence, the butting surfaces of the blanks are grounded and polished to remove stains and achieve absolute evenness. It is followed by alkaline cleaning with 50% NaOH solution and then by solvent (acetone) cleaning.

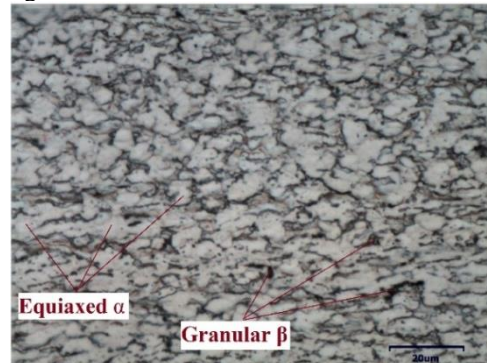


Fig. 1 Base material microstructure

All the cleaning processes were performed immediately before clamping and welding. A rigid clamping to base materials was provided to prevent distortion after welding. A Plasma arc welding machine with a TransTIG 4000 power source equipped with a plasma module was used in this investigation as it is shown in Figure 2 (a). Two gas cylinders comprising high purity argon (99.99% pure) are used to provide supply as plasma gas and primary shielding gas. A separate argon gas cylinder was employed to provide secondary shielding for protecting the top surface (trail shielding) and bottom surface (back purging) of the weld. The trail shielding and back purging supplies are shown in Figure 2 (b) and (c).



Fig. 2 Experimental setup

As this investigation was aimed to analyze the influence of plasma gas flow rate (PGFR) on the weld characteristics all the other parameters namely welding current, welding speed, arc length and other gas flow rates were kept constant (Welding Current – 65 A; Welding speed – 150 mm/min; Constricted Arc length – 7 mm) during all the welding experiments. The PGFR was varied between 0.6 L/min and 1 L/min with an interval of 0.1 L/min. The top and the bottom surface of the weld bead are shown in Figure 3. After welding, specimens were extracted for the analysis of the defect formation, microstructural characteristics and mechanical properties. All tension test specimens and specimens for metallography were sectioned perpendicular to the weld seam using wire-cut EDM.

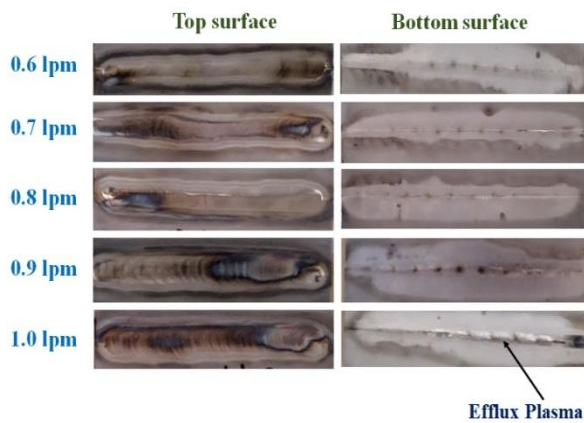


Fig. 3 Bead appearance

All the specimens were extracted using a wire-cut EDM process in order to prevent or minimize the risk of heat accumulation on the cutting surfaces which alters the microstructures and thereby mechanical properties. The extracted specimen for microstructure and macrostructure analysis consists of all the regions that include base material (BM), heat affected zone (HAZ) and fusion zone (FZ). The microstructures and macrostructures were captured using Huvitz Optical Microscope and Carl Zeiss Stemi 305 Stereo Zoom Microscope respectively. The scanning electron microscopy (SEM) was performed using JEOL equipped with energy dispersive spectroscopy (EDS). The tensile test was performed using a 100kN servo-controlled Universal testing machine (UTM) with a crosshead speed of 1 mm/min. Vickers microhardness test was performed using Shimadzu Vickers Hardness Tester and the hardness readings were recorded at an interval of 100 μm with a 200gf load.

3. Results and Discussion

3.1. Weld Geometry

The cross-section of the plasma arc welded $\text{Ti}_6\text{Al}_4\text{V}$ alloy joints to reveal the bead morphologies through macroscopic examination. Figure 4 helps to observe the morphologies of weld geometry like the width of the bead, penetration, heat affected zone area and fusion zone area.

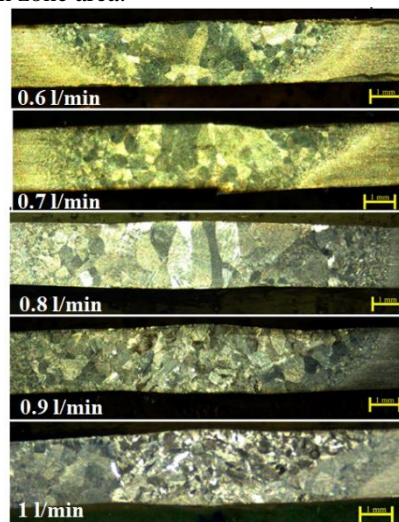


Fig. 4 Macrostructure

The macrographs reveal joints fabricated with 0.6 L/min and 0.7 L/min joints had a lack of penetration, while 0.8, 0.9 and 1 L/min joints had fully penetrated joints. The joints with complete penetration are desired criteria for the specimens to be analyzed further for the evaluation of tensile properties.

3.2. Tensile Properties

Tensile testing was conducted for the joints fabricated with complete penetration, i.e. joints with 0.8, 0.9 and 1 L/min. The tensile properties such as yield strength (YS), % elongation (%E), and ultimate tensile strength (UTS) were evaluated and the influence of PGFR on the tensile properties of the PAW $\text{Ti}_6\text{Al}_4\text{V}$ joints is shown in Figure 5. The results of tensile tests show that the tensile strength increase with the increase in PGFR whereas % elongation decreases with an increase in the PGFR. There are variations in the fracture locations in the tensile tested joints. The fracture location of the 0.8 L/min joints is at the base material whereas, in 0.9 and 1 L/min joints, it is at the FZ. The fracture surfaces are analyzed through SEM and EDS and the results are shown in Figure 6. The tensile properties of the welded joints are closely associated with the microstructure present in the FZ. Both the strength and ductility trends are strongly

justified by the microstructure as the formation of α -case causes embrittlement in the 1 L/min joint with high strength properties. The ductility of the joints reduces from 6.3% to 2.4% in the 0.8 and 1 L/min joints. The fracture surfaces of the tensile tested specimen were examined with SEM/EDS for analyzing the presence of porosity and compositional changes, which is shown in Figure 6.

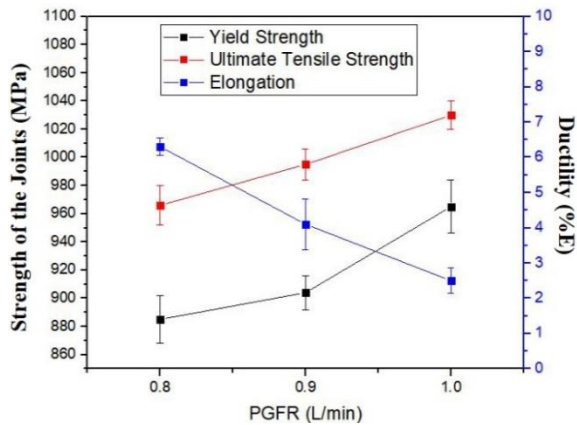


Fig. 5 Mechanical properties of welded joint

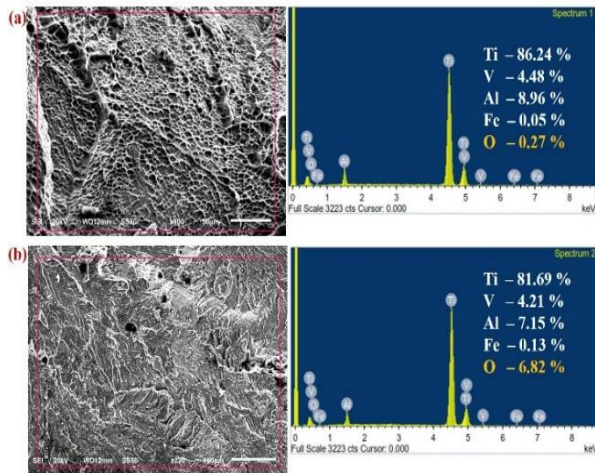


Fig. 6 Fracture surfaces of welded joint

In that Figure 6 (a) has a large population of dimples which is associated with the ductile mode of fracture whereas Figure 6 (b) is seen with cleavages and dark pore spots which contributed to the brittle failure. The fracture location in the 0.8 L/min joints is found in the base material whereas it is in FZ in the 1 L/min joint.

3.3. Microstructural Characteristics

The microstructure of the plasma arc welded Ti6Al4V alloy joints are shown in the Figure 7. The microstructures clearly reveal the FZ, HAZ, BM, FZ/HAZ interface and HAZ/BM interface. The FZ microstructure was characterized by the formation of prior β grains whereas HAZ microstructure was characterized by the presence of short needle like acicular martensite structures on the region between BM and FZ. It is observed that the grain size of the prior β grain structure gradually decreases towards the HAZ. Meanwhile the gradual reduction in grain size HAZ is also observed. The SEM/EDS results of the welded joints are shown in the Figure 8. In Figure 8, the composition of the FZ is found with increased amounts of oxygen in the case of 1 L/min joint while 0.8 and 0.9 L/min joints show negligible amounts.

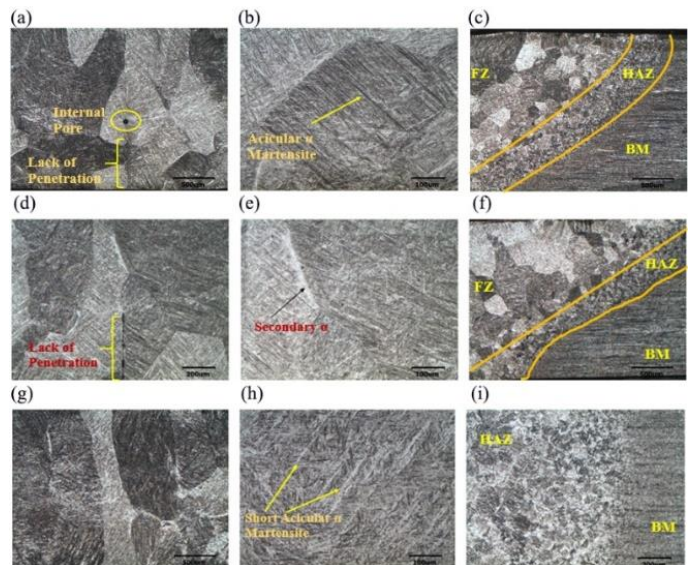


Fig. 7 Microstructure of plasma arc welded Ti-6Al-4V joints (a,b,c) Microstructure of Ti-6Al-4V joints for 0.6 L/min (d,e,f) Microstructure of Ti-6Al-4V joints for 0.7 L/min (g,h,i) Microstructure of Ti-6Al-4V joints for 0.8-1 L/min

The fusion zone of welded titanium alloy joints are majorly influenced by its microstructure that is generally characterized by prior β grains, presence of primary α , grain boundary α (secondary α) and acicular α martensite. Since this is an allotropic material, during welding transformation occurs in two ways, one is by diffusional β to α transformation and other by diffusion less β to α' (martensite) transformation. The transformation is determined primarily by the cooling rate where the transformation begins at the liquidus temperature of 1371°C. The mechanical properties of the joints are determined by the quantity, size and morphology of the above said structural phases in the Ti6Al4V alloy welds. The specific properties of the

prior β grain structure are difficult to analyze as it composed of three major phases namely retained β , acicular α and lath α martensite structures. The bright regions in the Figure 7 (a), (f) and (g) are composed primarily of α based phases whereas in the dark regions along with α based phases retained β phases is presented. Thus, the grain size of the prior β grains is not directly associated with the microhardness but of mostly related with ductility as it can be improved by refining the grain size. In the 0.6, 0.7 and 0.8 L/min joints of the Figure 7, the presence of prior β grain structure with lamellar α microstructure is observed. The grain size is observed to be increased with increased PGFR mainly due to the prevailing conduction mode of arc in the 0.6 - 0.8 L/min joints.

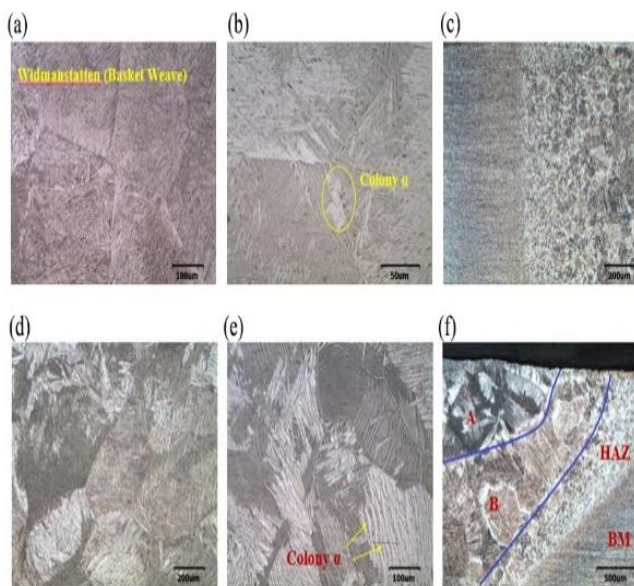


Fig. 8 (a,b,c) Microstructure of plasma arc welded Ti-6Al-4V joints for PGFR 0.9lm^{-1} (d,e,f) Microstructure of plasma arc welded Ti-6Al-4V joints for PGFR 1lm^{-1}

While the 0.9 L/min joint in the Figure 7, shows mixture of blocky α , acicular α and Widmanstätten α (basket weave) microstructures. In this particular joint the formation presence of α martensite is diminished. It is indeed the presence of α martensite is a sign of high cooling rate and also starting of the keyhole regime from conduction regime can also be differentiated by high cooling rate. Since there is a clear presence of basket weave structure in the microstructure it is confirmed that the keyhole mode of operation is not yet started in the case of 0.9 L/min joint. In Figure 5 (b), there is a presence of colonies of primary α in the grain boundaries which reinstate that the cooling rate is low for keyhole formation. Slow cooling of the weld bead is closely associated with the formation of secondary α or

grain boundary α which is detrimental to the tensile and fatigue properties of the joints. When keyhole is formed, the center of the weld pool experiences very high temperature rather than on the adjacent sides so that the heat is not allowed to dissipate widely and concentrates throughout the penetration. This is attributed to the striking of high pressure and stiff cylindrical arc on the workpiece.

According to the Figure 7 (f), a distinct layer of structure is formed in the FZ of the 1 L/min joint which is initially expected as colonies of Widmanstätten α structure as this structure is bright and bulky. But to thoroughly analyze the joint characteristics the layers are analyzed specifically. There was a suspicion that the layer formed on the sub surface of the joint could be a brittle layer known as α -case formed due to the high energy density dissolution of contaminants. The marking A in the Figure 7 (f) was identified as the layer of high dissolution of oxygen when examined through SEM/EDS analysis. The marking B in that microstructure was identified with negligible content of oxygen and characterized by the presence of a mixture of Widmanstätten α and acicular α martensite. The high dissolution of oxygen is confirmed through EDS which has a 9.79 % rise in the region of marking A compared to the region of marking B which shown in the Figure 6 (a) and (b).

In the Figure 7 (a) and (b) demonstrates the structures namely Widmanstätten α and α -case respectively in the 0.9 and 1 L/min joints. The α -case is an oxygen enriched brittle phase which is detrimental to the tensile and fatigue properties of the titanium alloys welded joints. This brittle subsurface layer is not desirable in case of welding operations but to avoid completely without a trace is also very difficult since even high purity shielding and plasma gases are generally having an average hydrogen and oxygen levels of 20 ppm.

3.4. Hardness

The hardness values of the various zones of the weld region were recorded using Vickers microhardness tester and the variation chart with respect to different PGFR are shown in the Figure 8. The hardness mapping shows the hardness values along the weld cross section which includes various regions of the weld such as FZ, HAZ and interfaces among them.

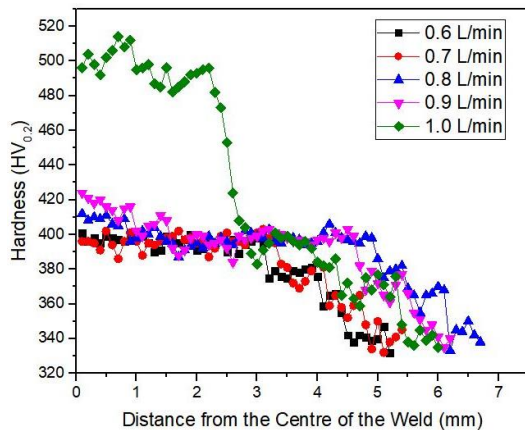


Fig. 8 Microhardness of welded joint

The highest hardness values were observed in the FZ which is followed by HAZ and BM irrespective of the variation in the PGFR. The hardness in the HAZ gradually decreases from near FZ to the BM. This gradual decrement in hardness was not observed in the case of FZ of the welded joints. Except 1 L/min joint, all the other joints exhibit the same hardness profile. In the case of 1 L/min joint, the hardness values spiked up to 545 HV which is the highest hardness recorded among all the joints. The average hardness of the base metal (Ti6Al4V) was found to be 342 HV. The peak hardness among the various zones of the weld zone is observed in the FZ irrespective of the variation in PGFR. All the FZ in the 0.6-0.9 L/min joints have a little variation of hardness in FZ as well as HAZ. The hardness in the HAZ gradually decrease from near FZ region to the BM (from 376 HV max. to 358 HV min) in all the joints. The presence of short acicular α martensite in the HAZ attributes to the increased hardness in the HAZ compared to BM. In 1 L/min joint, the peak hardness recorded in the FZ is 520 HV which is terribly high in case of titanium alloys attributed by the formation of α -case structures in the subsurface of the FZ. The α -case unaffected regions in the FZ of 1 L/min joint is having a peak hardness of 420 HV which is nominal (15% to 20% increase in hardness compared to BM).

4. Conclusions

- 1) The weld geometries such as width of bead, depth of penetration, fusion zone area, heat affected zone area increases with increase in plasma gas flow rate under conduction mode and the trend begins to reverse gradually as there is formation of keyhole.
- 2) The penetration of the weld increases with increase in PGFR as the increased rate of arc

deposition penetrates the surface leads to the formation of keyhole. The weld shape defects such as underfill and undercut were not observed.

- 3) The microstructure associated with cooling rate is affected by the plasma gas flow rate as the mode of PAW is changing from conduction to keyhole. Most microstructures are observed with acicular α martensite and Widmanstätten α structures.
- 4) The products of hard martensite phases at higher PGFR is due to the strength of the joints being directly related to the plasma gas flow rate.
- 5) The ductility of the joints has an inverse relationship with the PGFR where there was a 65% reduction observed at 1 L/min joint.

Acknowledgement

Authors wish to acknowledge Science and Engineering Research Board (SERB), Department of Science and Technology (DST) for the provision of Plasma Arc Welding (PAW) equipment through the funded project (DST File No. EEQ/2017/000339).

References

1. A.B. Short, *Gas Tungsten Arc Welding of $\alpha + \beta$ Titanium Alloys: A Review*, Mater. Sci. Technol., Taylor & Francis, 2009, 25(3), p 309–324.
2. A. V Lukoyanov, *Formation of Pores in the Weld Metal in Automatic Argon-Shielded Arc Welding of Titanium Alloys*, Weld. Int., Taylor & Francis, 2014, 28(4), p 301–303.
3. M. Peters, J. Hemptenmacher, J. Kumpfert, and C. Leyens, *Structure and Properties of Titanium and Titanium Alloys*, Titanium and Titanium Alloys, John Wiley & Sons, Ltd, 2003, p 1–36.
4. C. Leyens, "Oxidation and Protection of Titanium Alloys and Titanium Aluminides," Titanium and Titanium Alloys, 2003, p 187–230.
5. H. Sibus, "Titanium and Titanium Alloys – From Raw Material to Semi-Finished Products," Titanium and Titanium Alloys, 2003, p 231–244.
6. M. Peters, J. Kumpfert, C.H. Ward, and C. Leyens, *Titanium Alloys for Aerospace Applications*, Adv. Eng. Mater., 2003, 5(6), p 419–427.
7. D.I. Pantelis, M. Kazasidis, and P.N. Karakizis, *Titanium Alloys Thin Sheet Welding with the Use of Concentrated Solar Energy*, J. Mater. Eng. Perform., 2017, 26(12), p 5760–5768.
8. I. Balasundar, T. Raghu, and B.P. Kashyap, *Correlation between Microstructural Features and Tensile Properties in Near- α Titanium Alloy IMI 834 Processed in the $\alpha + \beta$ Regime*, Mater. Perform. Charact., G.E. Totten, Ed., (West

- Conshohocken, PA), *ASTM International*, 2019, 8(5), p 932–945.
9. M. Peters, J. Kumpfert, C.H. Ward, and C. Leyens, *Titanium Alloys for Aerospace Applications*, *Adv. Eng. Mater.*, 2003, 5(6), p 419–427.
 10. M.A. Vasechkin, O.Y. Davydov, A.B. Kolomenskii, and S. V Egorov, *Effect of Welding and Heat Treatment Regimes on the Mechanical Properties of Various Titanium Alloy Welded Joints*, *Chem. Pet. Eng.*, 2018, 54(7), p 525–530.
 11. M. Baruah and S. Bag, *Microstructural Influence on Mechanical Properties in Plasma Microwelding of Ti6Al4V Alloy*, *J. Mater. Eng. Perform.*, 2016, 25(11), p 4718–4728.
 12. M. Vyskoč, M. Sahul, and M. Sahul, *Effect of Shielding Gas on the Properties of AW 5083 Aluminum Alloy Laser Weld Joints*, *J. Mater. Eng. Perform.*, 2018, 27(6), p 2993–3006.
 13. P. Kumar and A.N. Sinha, *Effect of Heat Input in Pulsed Nd:YAG Laser Welding of Titanium Alloy (Ti6Al4V) on Microstructure and Mechanical Properties*, *Weld. World*, 2019, 63(3), p 673–689.
 14. J. CHEN and C. PAN, *Welding of Ti-6Al-4V Alloy Using Dynamically Controlled Plasma Arc Welding Process*, *Trans. Nonferrous Met. Soc. China*, 2011, 21(7), p 1506–1512.
 15. W. Sun, M. Mohammed, L. Xu, T. Hyde, D. McCartney, and S. Leen, *Process Modelling and Optimization of Keyhole Plasma Arc Welding of Thin Ti-6Al-4V*, *J. Strain Anal. Eng. Des.*, 2014, 49, p 410–420.
 16. A. Deshpande, A. Short, W. Sun, D. McCartney, L. Xu, and T. Hyde, *Finite Element-Based Analysis of Experimentally Identified Parametric Envelopes for Stable Keyhole Plasma Arc Welding of a Titanium Alloy*, *J. Strain Anal. Eng. Des.*, 2012, 47, p 266–275.
 17. S. Sundaresan and G.D.J. Ram, *Use of Magnetic Arc Oscillation for Grain Refinement of Gas Tungsten Arc Welds in α - β Titanium Alloys*, *Sci. Technol. Weld. Join.*, Taylor & Francis, 1999, 4(3), p 151–160.
 18. T.R. Muth, Y. Yamamoto, D.A. Frederick, C.I. Contescu, W. Chen, Y.C. Lim, W.H. Peter, and Z. Feng, *Causal Factors of Weld Porosity in Gas Tungsten Arc Welding of Powder-Metallurgy-Produced Titanium Alloys*, *JOM*, 2013, 65(5), p 643–651.
 19. V.I. Murav'ev, R.F. Krupskii, R.A. Fizulakov, and P.G. Demyshev, *Effect of the Quality of Filler Wire on the Formation of Pores in Welding of Titanium Alloys*, *Weld. Int.*, Taylor & Francis, 2008, 22(12), p 853–858.
 20. T.S. Balasubramanian, M. Balakrishnan, V. Balasubramanian, and M.A. Muthu Manickam, *Effect of Welding Processes on Joint Characteristics of Ti-6Al-4v Alloy*, *Sci. Technol. Weld. Join.*, 2011, 16(8), p 702–708.
 21. V.P. Leonov, V.I. Mikhailov, I.Y. Sakharov, and S. V Kuznetsov, *Welding of High-Strength Titanium Alloys of Large Thicknesses for Use in Marine Environments*, *Inorg. Mater. Appl. Res.*, 2016, 7(6), p 877–883.
 22. W.D. Brewer, R.K. Bird, and T.A. Wallace, *Titanium Alloys and Processing for High Speed Aircraft*, *Mater. Sci. Eng. A*, 1998, 243(1), p 299–304.